JOURNAL OF MATERIALS SCIENCE 29 (1994) 5515–5523

Simulation of disruption loads on first-wall high-temperature materials

K. WETZIG, S. MENZEL, U. ROSSEK
Institut für Festkörperanalytik und Strukturforschung im Institut für Festkörper- und Werkstofforschung, Dresden e. V., Postfach, 01171 Dresden, Germany

B. SCHULTRICH
Fraunhofer-Einrichtung für Werkstoffphysik und Schichttechnologie Dresden, Postfach, 01171 Dresden, Germany

The behaviour of carbon materials under thermal load in fusion reactors has been simulated by laser-pulse irradiation in a scanning electron microscope (SEM). In this way material damage, such as thermal shock crack formation and propagation, and erosion behaviour, can be studied *in situ* in the SEM with high lateral resolution. The dependence of damage initiation and propagation on the laser-beam parameters (pulse number, energy, spot size, spot duration and energy density), is of special interest. The damage behaviour is strongly determined by special materials structures. Because of its fibre reinforcement, the investigated CFC composite materials proved to be more stable to erosion and crack formation than homogeneous fine-grained graphites. High-temperature damage may be diminished by the use of carbon materials with creep-resistant components.

1. Introduction

Materials behaviour under thermal shock load is of basic interest for many applications, especially in the field of energy production. An exceptionally high load exists in the first wall of fusion reactors during plasma disruptions. At these plasma instabilities, the magnetic plasma shield will be disrupted and the plasma energy will be deposited on the first wall within a few milliseconds. With it, an energy density of some MJ m^{-2} can be reached at the strongest loaded components, that is the divertor or the limiter, respectively [1, 2]. Of the possible high-temperature materials suitable for these critical components, carbon materials are preferred at present. They possess a low atomic number, favourable to a low influence of evaporated material on the plasma, and also a sufficient thermoshock and erosion strength. Two different material classes compete here: fine-grained graphites and carbon fibre-reinforced carbons (CFC). The CFC materials combine a relatively high strength with an excellent thermal conductivity in certain directions. On the other hand, both the anisotropy of fibre reinforcement and the heterogeneous structure of fibres and the surrounding matrix provide difficulties for modelling. Compared with this, fine-grained graphites are much more isotropic concerning their structure and materials behaviour. Extensive experience in their application exists in the field of high-temperature reactor techniques. Disruption loads cause structure damage, crack formation and material erosion by evaporation or microablation. The thermal conditions can be advantageously simulated by means of high-power pulse lasers. The damage mechanisms are studied by investigations in the submicroscopic range with special attention to crack formation and propagation processes and to localized cumulative effects under multiple shock load. The experimental investigations were carried out with a new expressive method, by which the surface topography variation of a certain microscopic area can be observed with high lateral resolution. For this purpose, a special apparatus combination (LASEM) was developed, which enables *in situ* laser irradiation inside a scanning electron microscope [3, 4]. Representative typical carbon materials, a fine-grained graphite (EK 98, Ringsdorff GmbH) and a carbon fibre-reinforced composite material (FMI, Composites Ltd), were investigated.

2. Experimental conditions

The simulation experiments were carried out in a scanning electron microscope combined with a high-power pulse laser. The apparatus allows the following experimental possibilities:

(i) repeated series of laser irradiation and SEM images of the same microscopic area,

(ii) investigation of cumulative damage effects after multiple laser irradiation with a high lateral resolution,

(iii) avoidance of environmental influences by high-vacuum conditions at the sample stage.

Fig. 1 shows the experimental apparatus (LASEM) schematically. The used Nd–YAG laser ($E_{max} = 10$ J, $\tau \approx 5$ ms, $f = 1$ Hz) is inserted into the vacuum cham-

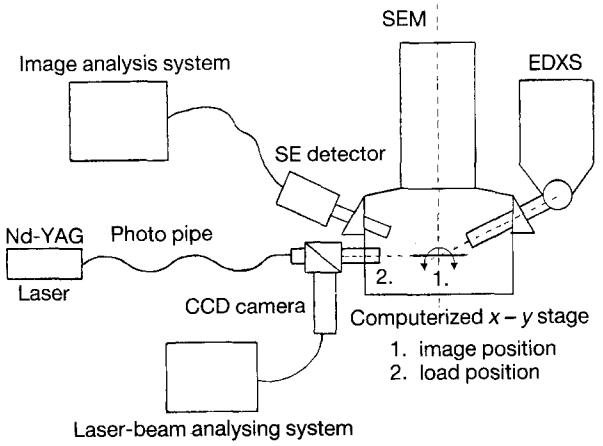

Figure 1 Schematic representation of the experimental apparatus (LASEM).

ber of the SEM by means of a gradient photo pipe with a coupling, and focusing optics and a coupling module. The laser-beam energy can be reproducibly changed by an optical filter set. A CCD camera in connection with a laser-beam analysing system allow the measurement of the beam parameters and of the energy density profile in the laser beam. Both the attainable energy density, $q_{max} > 10\ J\,mm^{-2}$, and the pulse duration, $\tau = 5$ ms, are of the order of the required values for a simulation of disruption conditions in the reactor ($q = 1$–$10\ J\,mm^{-2}$, $\tau = 2$–10 ms) [1].

With the described experimental apparatus, damage effects (crack formation, material erosion) were investigated, which occurred on unpolished and polished surfaces of fine-grained graphite EK 98 and CFC material FMI after laser irradiation. The results discussed below were obtained by varying the parameters laser pulse energy, spot area and pulse number. Furthermore, the ion-beam slope cutting technique (after Hauffe and Schultrich [5]) and image processing methods [6] were used for the study of damage structures.

3. Results

3.1. Surface topography

The fine-grained graphite EK 98, which shows a largely isotropic materials behaviour was investigated. On the polished surfaces the laser spot is marked by a distinct increase of the surface porosity (Fig. 2a). EK 98 possesses a relatively high open porosity of about 10%. By using the polishing process, pores visible at the surface become covered or loosely filled.

The impinging radiation causes an increase of the surface temperature, and therefore the pressure of the included gas also increases. Because of that, tensile stresses of the order of $(D/h)\ p$ (D = pores dimension, h = cover layer thickness, p = inside pressure) develop in the thin cover layer. Simultaneously, because of the thermal isolation by lower pores situated, the cover layer suffers a strong local overheating in the order of l_{th}/h, ΔT (thermal penetrating depth $l_{th} = (a\tau)^{1/2} \approx 0.3$ mm, with thermal diffusion coefficient

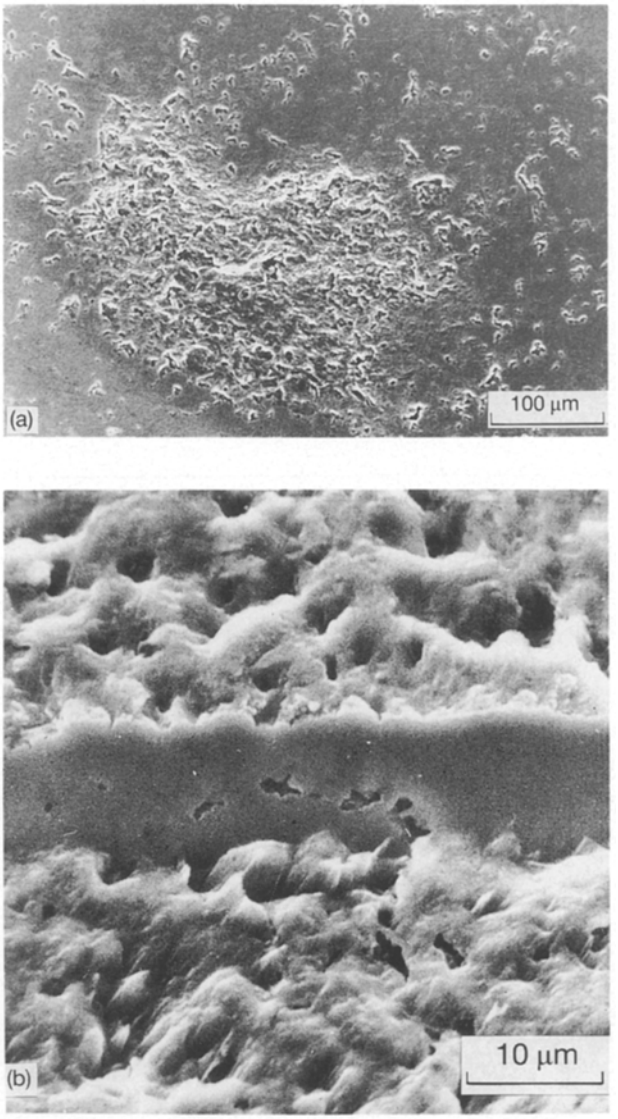

Figure 2 Porosity of graphite EK 98 after laser irradiation with $\bar{q} \approx 0.3\ J\,mm^{-2}$, $\varphi = 45°$, $N = 1$ pulse, unpolished surface: (a) surface porosity; (b) ion-beam slope cutting profile (after Hauffe and Schultrich [5]).

$a \approx 10\ mm^2\,s^{-1}$), compared with the mean surface temperature increase, ΔT. The interplay of the inside pressure and a temperature-determined decrease of the deformation resistance, may cause an opening of the covered pores. As a result, the surface porosity grows with increasing laser energy density. The depth profile through a laser spot (Fig. 2b) shows an enhanced pore density below the laser-irradiated surface, because of the expansion of included gases, which have not yet erupted to the surface.

3.2. Thermal shock cracks

First the results for fine-grained graphite EK 98, a material with a distinctly isotropic behaviour (see Section 3.1) will be discussed. That part of the depth profile below the laser-irradiated surface shows not only an enhanced pore density, but also some thermal shock cracks (Fig. 3a) and therefore an enhanced inclination for ablation (Fig. 3b).

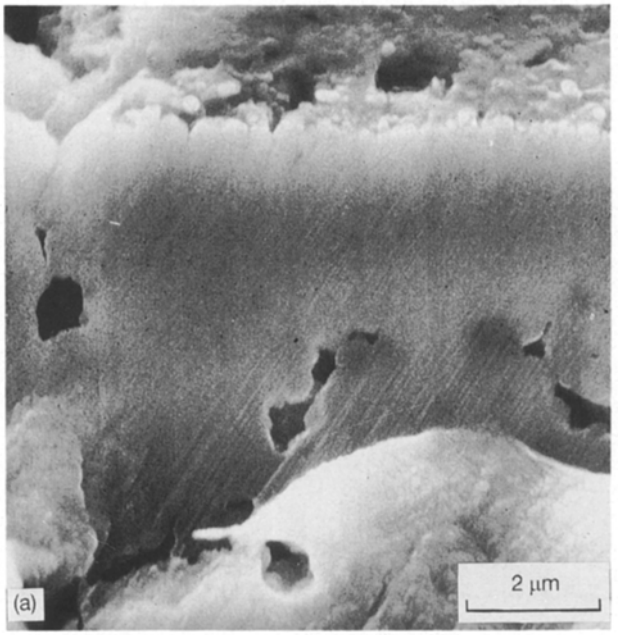

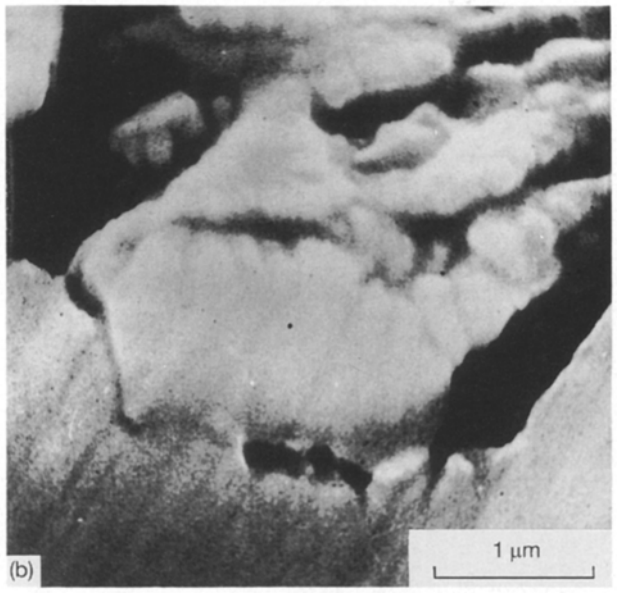

Figure 3 Ion-beam slope cutting [5] through a laser spot on graphite EK 98: (a) thermal shock crack below the surface ($\bar{q} \approx 0.3\,\mathrm{J\,mm^{-2}}$, $\varphi = 45°$, $N = 1$ pulse); (b) microparticle ablation by crack formation ($\bar{q} \approx 0.5\,\mathrm{J\,mm^{-2}}$, $\varphi = 45°$, $N = 1$ pulse).

An overview of the dependence of possible crack formations on the irradiation conditions is given in Fig. 4. For the purposes of a "damage map", Fig. 4 shows the observed types of damage in a plane given by the mean energy density, $\bar{q} = E/A_{sp}$ versus the spot area, A_{sp}, characterizing the irradiation conditions. The appearance of thermal shock cracks requires a critical threshold value of the energy density. Crack formation occurs in the field of full points of measurement. The different lateral distribution of laser energy density on the sample surface causes a dependence of critical crack conditions not only on the mean laser energy density, $\bar{q}$, but also on the spot area, A_{sp}, and consequently on the energy density gradient. At a constant laser energy, the energy density gradients of beam cross-section grow with increasing focusing.

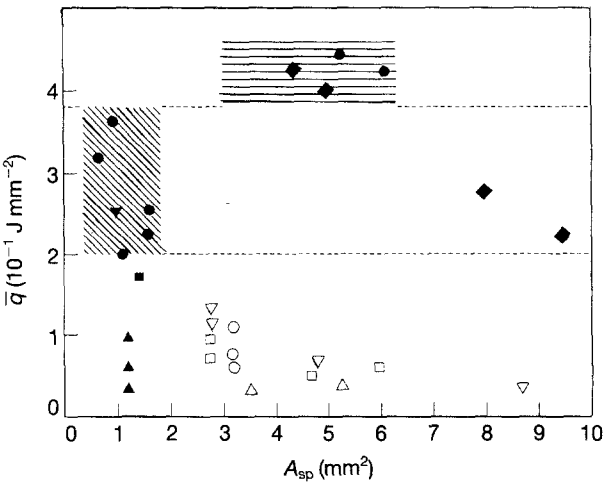

Figure 4 Critical laser energy densities, $\bar{q}$, for crack formation in irradiated graphite EK 98: (●, ◆) full energy density; (▽, □, △) increasing beam weakening by dimming); full points, crack formation; (\\\\) lamellar structure, (——) macroscopic cracks.

Above a critical spot area, no thermal shock cracks could be observed even at higher energy densities, because the required temperature gradients on the materials surface were not reached (Fig. 4). Beyond a threshold energy density value of about $0.2\,\mathrm{J\,mm^{-2}}$, lamellar crack structures are visible in the range of potential crack formation, which are generated by a layer splitting under tensile stress in the cooling phase. Because of a preferred binder phase evaporation, the morphology of graphite grains is increasingly visible.

By crack growth processes, microcracks with dimensions of some micrometres, mainly generated in the binder material, can form special macroscopic crack networks for energy densities above $\bar{q}_{crit} = 0.4\,\mathrm{J\,mm^{-2}}$, which may be evaluated for their characteristic values by means of image processing [6]. As an example Fig. 5 gives the branch lengths, the distribution of distances between branches, and branch length weighted orientation of thermal shock cracks on graphite EK 98. At a beam incidence angle of 45°, a preferred crack orientation exists in the direction of the minimal diameter of the elliptical spot area.

The thermal shock crack behaviour of CFC composite material FMI is considerably determined by its heterogeneous and anisotropic microstructure. It consists of carbon fibres of about 10 μm diameter, embedded in a graphitic matrix. The fibres are integrated in bundles with about 1 mm thickness and aligned in one of four preferred orientations. The microstructure anisotropy cause an anisotropic damage behaviour. As proof of this, only single fibre bundles with a given orientation are irradiated by the laser beam at a time. Laser-beam loading occurred perpendicular as well as parallel to the fibre axis. A characteristic of this material is that microcrack growth occurs in the binder (Fig. 6a). Multiple laser-beam load results in a formation of macroscopic cracks and in their spreading near the phase boundary between binder and fibre (Fig. 6b). The higher resistant fibres cause a "diversion" of the crack-growth direction. In this way the materials fracture toughness will be enhanced. An analogous effect

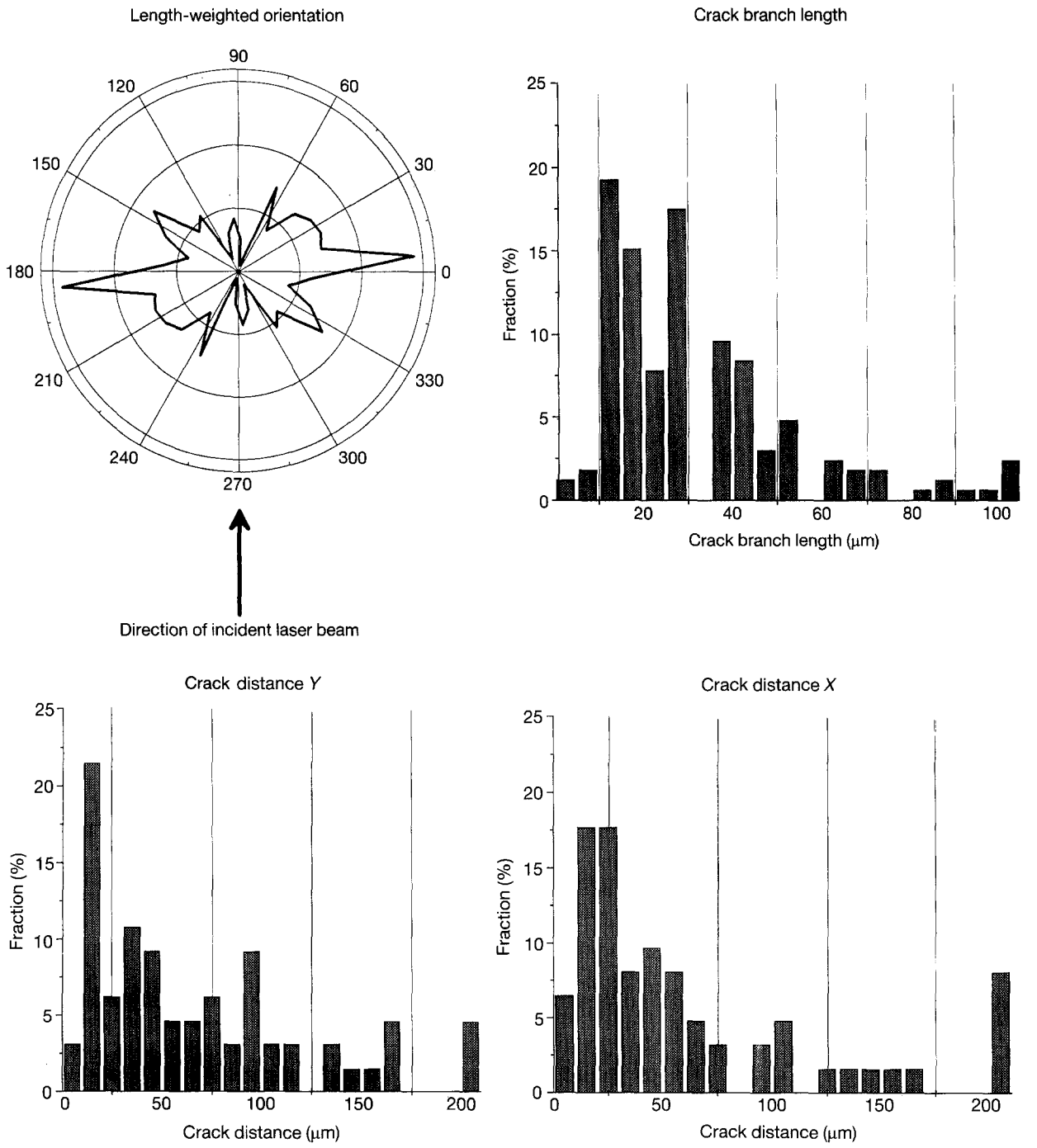

Figure 5 Quantitative image analysis of thermal shock cracks on graphite EK 98 after laser irradiation ($\bar{q} = 1.0\,\mathrm{J\,mm^{-2}}$, $N = 1$ pulse, $A_{sp} = 5.2\,\mathrm{mm^2}$, $\varphi = 45°$).

in the macroscopic range is caused by an orientation change of the embedded fibre bundles.

Fig. 7 shows crack growth after 1 and 100 laser pulses. The material was irradiated parallel to the fibre axis. Under the present load conditions ($\bar{q} \approx 1.5\,\mathrm{J\,mm^{-2}}$) a first radially running macroscopic crack is visible even after one pulse (Fig. 7a). Under high load values, radial cracks in the fibre cross-section could be observed, by which high fibre residual stresses were diminished. Above $0.4\,\mathrm{J\,mm^{-2}}$, transversely ruptured fibres appeared here and there.

3.3. Materials erosion

Under the present loading conditions, crack formation is superimposed by erosion processes. On the materials surfaces, characteristic erosion craters develop, the profile of which depends on both the energy density distribution in the laser beam (Fig. 8a) and the materials structure. Fig. 8b shows the maximal erosion depth, $t_{E_{max}}$, of the erosion craters on graphite EK 98 for different energy density values. At $\bar{q} = 1.2\,\mathrm{J\,mm^{-2}}$, the focused laser beam generates erosion depths of 100 μm per pulse, almost independent of the materials orientation. Multiple load results in saturation of erosion, which could be caused by different processes. Possibilities for it are a variation of surface properties, the observed redeposition of vaporized material in the spot area, an increase of the effective irradiated surface and from it a fall below the critical energy density, or a change of the erosion mechanism.

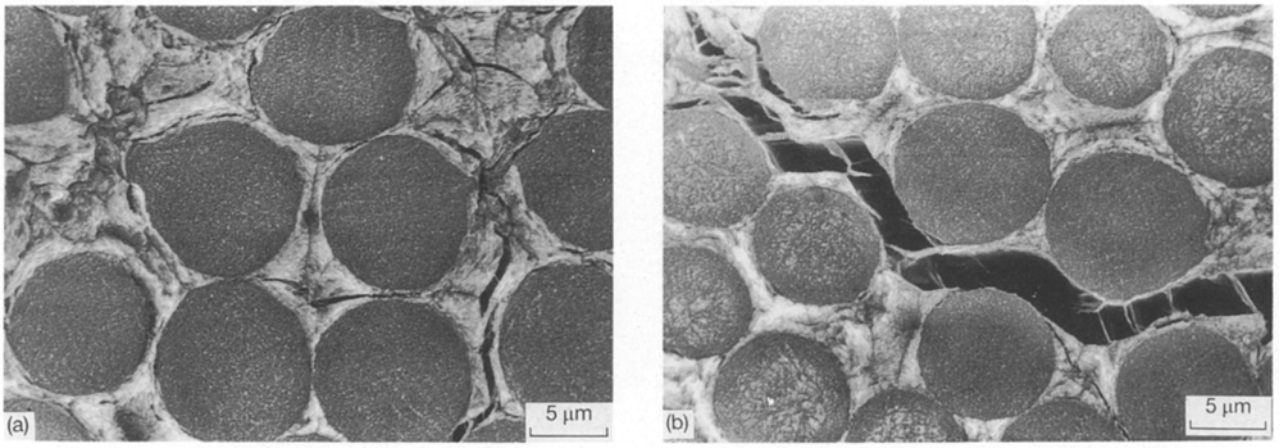

Figure 6 Thermal shock cracks in CFC material FMI after laser irradiation, $\varphi = 0°$, unpolished surface; (a) parallel to the fibre axis ($N = 1$ pulse, $\bar{q} = 0.8\ \mathrm{J\,mm^{-2}}$); (b) parallel to the fibre axis ($N = 2$ pulses, $\bar{q} = 1.5\ \mathrm{J\,mm^{-2}}$).

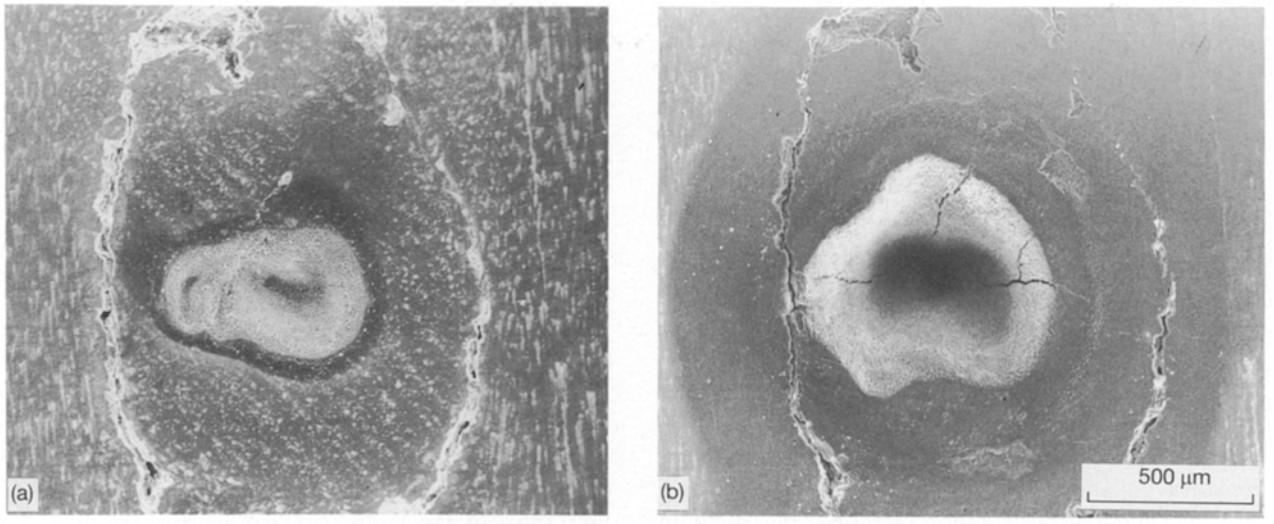

Figure 7 Multiple laser irradiation of composite material FMI with $\bar{q} = 1.5\ \mathrm{J\,mm^{-2}}$, $\varphi = 0°$, unpolished surface; (a) after 1 pulse; (b) after 100

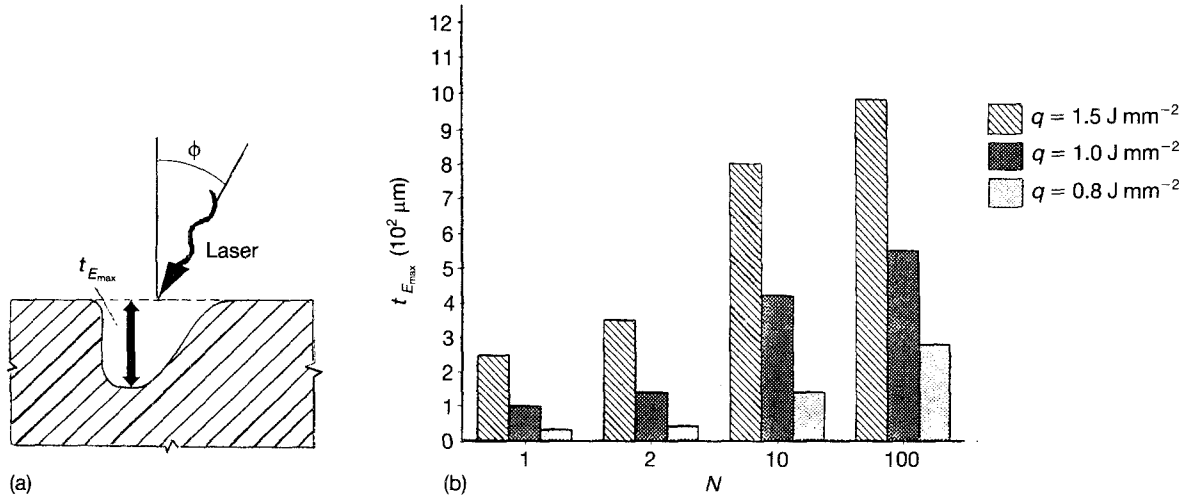

Figure 8 Material erosion by laser irradiation of unpolished graphite EK 98 surface; (a) erosion profile (schematic drawing); (b) maximum depth, $t_{E_{max}}$, of erosion craters as a function of laser pulse number, N, and energy density, $\bar{q}$, at a constant energy $E = 6$ J, $\varphi = 0°$.

Fig. 9 shows the erosion of an unpolished surface of graphite EK 98 after multiple laser irradiation. A similar saturation effect of the erosion process is observed after repeated electron-beam bombardment [1, 8].

High pulse numbers cause deposition layers near the crater edge, by which earlier generated cracks may be covered. Outside the erosion craters, evaporated material is deposited in the form of about 10 μm-sized particles.

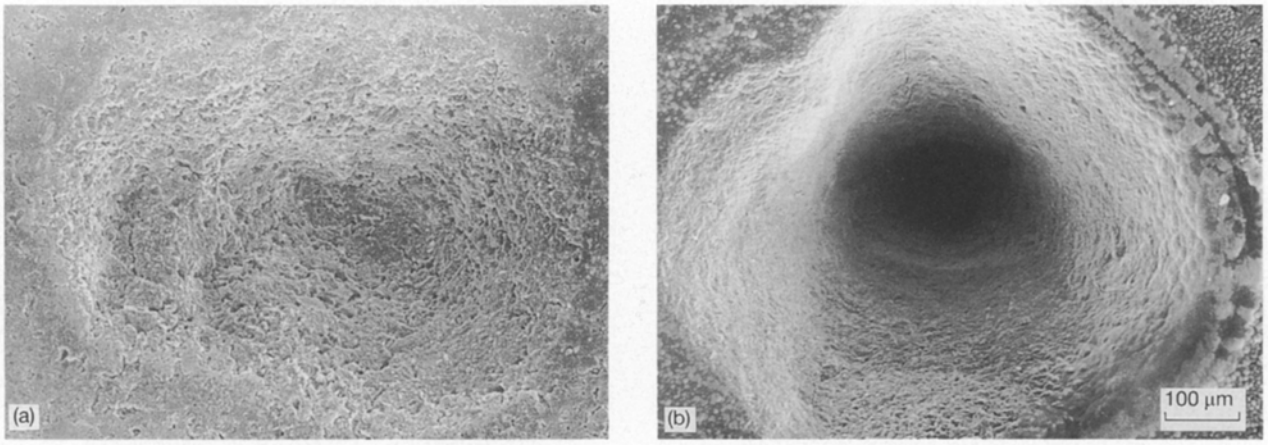

Figure 9 Erosion at unpolished graphite EK 98 surfaces ($\bar{q} = 1.0\ \mathrm{J\,mm^{-2}}$, $\varphi = 0°$); (a) after 1 pulse; (b) after 100 pulses.

For the composite material FMI, material erosion under strongly localized loads depend on the beam direction relative to fibre orientation. At a perpendicular irradiation, the enhanced thermal conductivity of fibres compared with the binder causes an anisotropic extension of the temperature field with a preferred lateral extension. As a result, the observed craters are wide but shallow, compared with those after an axial irradiation. Therefore, the erosion profile after large area load of fibre bundles differs from the energy profile in the laser beam.

Corresponding to the heterogeneous structural conditions, binder and fibres show a different erosion behaviour (Fig. 10). For relatively low energy densities, binder material, as expected, will be more strongly eroded than fibres. On the other hand, for high energy densities the binder towers above fibre ends. These opposite tendencies are compensated for medium irradiation densities, i.e. flat surfaces will remain. These dependences of surface structure on irradiation conditions are important points in the understanding of the appearance of stresses and deformation (see Section 4).

Fig. 11 shows the maximum erosion depth, $t_{E_{max}}$, for parallel and perpendicular laser irradiation of one fibre bundle as a function of the laser pulse number, N. At perpendicular irradiation, generally higher erosion rates are observed. As with graphite EK 98, the material evaporated per pulse diminishes under multiple load, i.e. we again have a saturation of the erosion behaviour.

4. Discussion

4.1. Thermal shock cracks

Both the formation and growth of thermally induced cracks are mainly caused by tensile stresses, which can be produced by two different mechanisms: either exclusively in a thermoelastic manner or assisted by creep relaxation. In the latter case, stresses reverse in a certain way compared with the thermoelastic case. Two parts of a solid, bordering on each other and possessing the same initial temperature, expand by laser irradiation to different extents, if they have varying expansion coefficients or a differing final heat-up temperature. In the less-expanded part (by a lower expansion coefficient or lower heat-up temperature) tensile stresses develop, from which cracks may be generated. At higher temperatures with considerable creep processes, such stresses may be reduced by viscous creep without crack formation. During the subsequent cooling process, the stronger expanded part also tries to shrink to a stronger extent. However, this will be prevented by the less-contracted bordering parts, and therefore permanent tensile stresses develop in the stronger expanded parts, which may again give rise to crack formation, especially to circumferential cracks at spot edges (Figs 7 and 9). Different expansion coefficients may be caused by the heterogeneous structural conditions or by the strong anisotropy of graphite grains. Lateral temperature differences are caused by inhomogeneous irradiation (especially the limitation of the irradiation spots) and by different thermal conductivities of the individual structural components.

The thermoelastic forces during heat up thermoshocks will produce only compressive stresses at the surfaces, if additional effects, such as irradiation inhomogeneities or structural anisotropy, are disregarded. However, the observed crack formations cannot be explained by this. Compressive stresses, though, will be reduced by creep processes in the high-temperature phase and converted into tensile stresses during subsequent cooling down. In the case of carbon composite material with its distinct structural heterogeneity, the activity of this mechanism, which otherwise is hardly detectable, can be immediately verified (Fig. 10). At low irradiation intensities, as expected, the binder material will be more strongly eroded than the fibres, which therefore will rise above the surface. For higher intensities, the complementary surface topography develops. During the heating process, compressive stresses are formed, which press the binder material out from the surface. On subsequent cooling, the material will shrink, and therefore wide-opening cracks develop. From the sharp-edged binder areas it can be seen that this behaviour is not caused by an inversion of selective erosion. Also, the crack network anisotropy in spot ellipses can be explained by a stronger creep relaxation and, therefore, a stronger

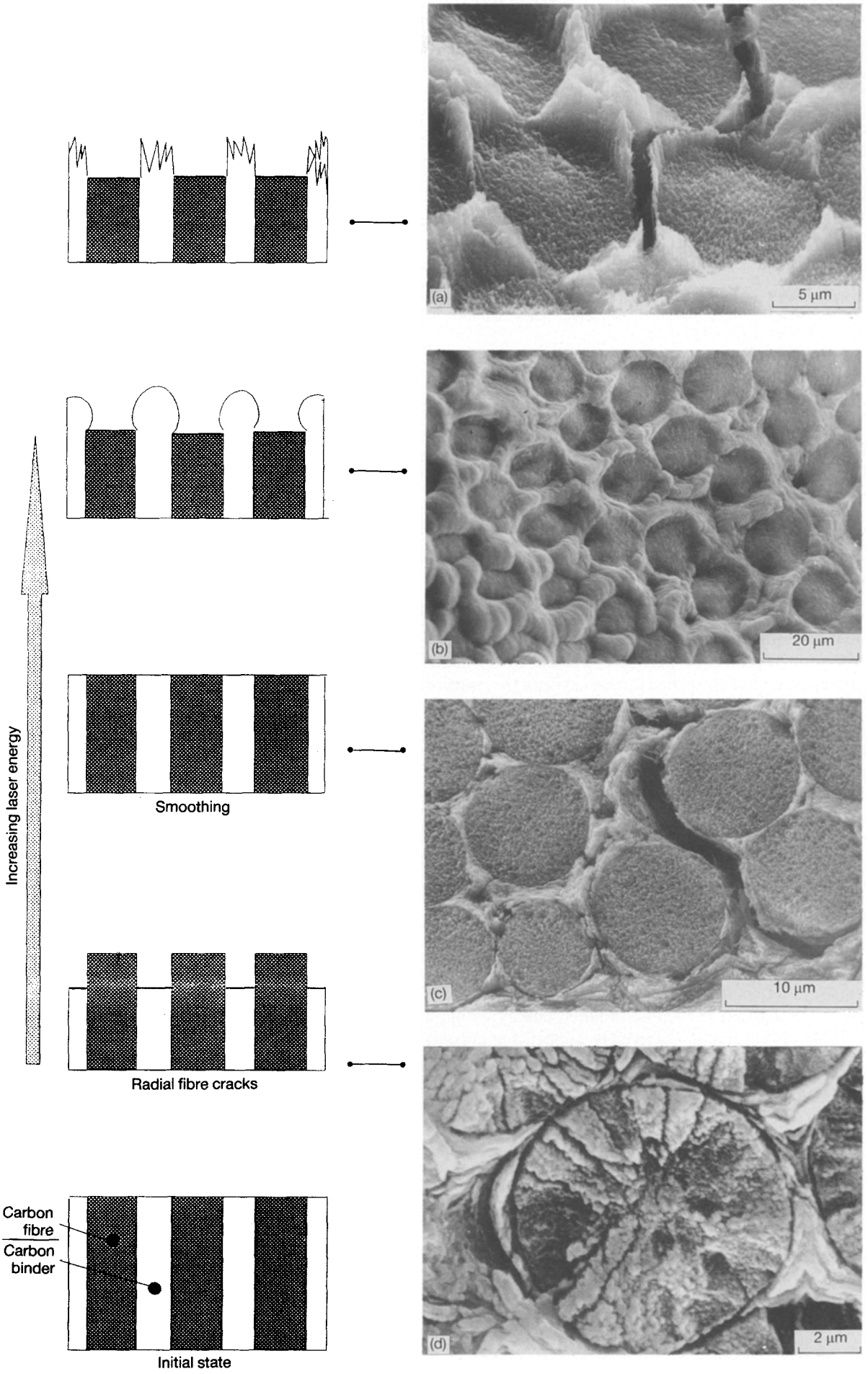

Figure 10 Qualitative damage behaviour of CFC composite material FMI after laser irradiation. Superposition of erosion with redeposition, thermal expansion, relaxation and thermal contraction in the spot region.

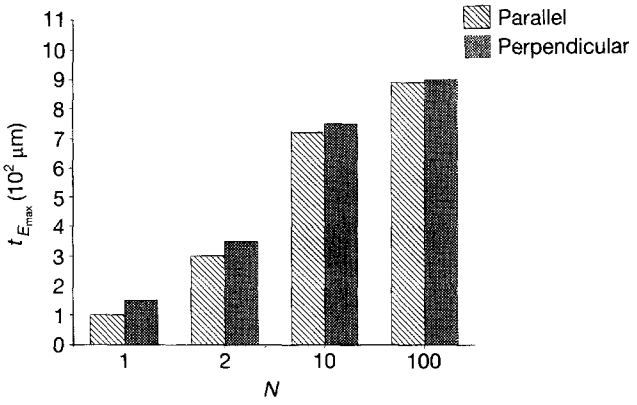

Figure 11 Maximum depth, $t_{E_{max}}$, of erosion craters on unpolished FMI surfaces as a function of laser pulse number, N ($\bar{q} = 1.5\,\mathrm{J\,mm^{-2}}$, $\varphi = 0°$).

tensile stress development in the direction of laser irradiation.

Additional crack structures are caused by irradiation inhomogeneity: macrocracks leave the spot centre radially outwards, and some of them turn into circumferential cracks surrounding the spot. This crack course corresponds very well with stress distribution obtained by high-temperature creep: inside the relaxed and shrunk spot area only tensile stresses exist. Near the spot edge, tensile stresses are found in the radial direction and compressive stresses exist in the rotation direction. The formation of circumferential cracks is additionally promoted by shearing stresses formed at spot edges by squeezing out of the central spot region.

4.2. Material erosion

The erosion of carbon materials by laser-pulse irradiation is usually explained by the evaporation of carbon atoms or molecules (C_2, C_3, ...). Because of the existence of carbon clusters, the specific sublimation heat, Q_v, is diminished to a value of $23\,\mathrm{kJ\,g^{-1}}$, compared with $60\,\mathrm{kJ\,g^{-1}}$ for atomic evaporation [2]. An estimation of the maximal erosion depth, $t_{E_{max}}$, can be made by assuming that the whole radiated energy within a cylindrical volume is completely applied for evaporation

$$t_{E_{max}} = \frac{q}{Q_v\,\rho} \qquad (1)$$

For a maximum energy density, $q = 3.2\,\mathrm{J\,mm^{-2}}$ ($\bar{q} = 1.5\,\mathrm{J\,mm^{-2}}$), a maximal erosion depth, $t_{E_{max}} \approx 70\,\mu\mathrm{m}$, results (with $\rho \approx 2\,\mathrm{g\,cm^{-3}}$). Experimentally, however, crater depths of more than 200 µm were found. Part of radiated energy that is available for evaporation is also reduced by reflection and thermal conduction losses.

Similar discrepancies also exist for the dependence of erosion on the irradiation conditions [8]. The enhanced erosion may be caused by erosion not only of carbon molecules but also of whole microparticles instead of an atomic evaporation. Such microparticles with dimensions of about 10 µm are an essential part of the material deposited near erosion crater edges. The microparticles may be lost because thermal shock cracks give rise to an increased thermal isolation and, as a result, to an increased local heating. In this way, all damage process phenomena, such as surface topography, thermal shock cracks and erosion, are closely linked together.

5. Conclusions

Thermal shock loads of carbon materials which occur in fusion reactors have been simulated by laser-pulse irradiation in the SEM, and the material damage behaviour was investigated *in situ*. Different types of crack formation in fine-grained graphite (EK 98) and in carbon fibre-reinforced composite material (FMI) were investigated, and also using additional methods such as ion-beam slope cutting and quantitative image processing. Cracks are particularly caused by stress relaxation during high-temperature creep and by the resulting tensile stresses in the cooling phase. Material erosion depths exceed the values which may be expected for pure evaporation, by a factor 3. This can be explained by a dominant erosion in the form of microparticles, which are removed by thermal shock cracks. Such particles with sizes of about 10 µm play a considerable part in the formation of redeposition layers near the erosion crater edges. The observed erosion saturation will be caused by an exhaustion of particle erosion.

Because of its fibre reinforcement, the CFC composite material FMI proved to be much more stable to erosion and crack formation compared with the fine-grained graphite EK 98. The damage behaviour was strongly determined by surface pretreatment (such as polishing or preceding irradiation) and by load inhomogeneity. Therefore, simulation experiments should be realized under homogeneous irradiation conditions and with "steady state" surfaces. High-temperature damage may be reduced by the use of carbon materials with creep-resistant components.

Acknowledgements

This work is part of a project, task 03M20858, with financial support by Bundesminister für Forschung und Technologie. The authors are responsible for the contents.

References

1. J. LINKE, M. AKIBA, M. ARAKI, A. BENZ, H. BOLT, H. HOVEN, K. KOIZLIK, H. NICKEL, M. SEKI and E. WALLURA, in "Proceedings of the 16th Symposium on Fusion Technology", edited by B. E. Keen, M. Huguet, R. Hemsworth (Elsevier, B.V, Amsterdam, 1991) p. 428.
2. J. G. van der LAAN, *J. Nucl. Mater.* **162–164** (1989) 964.
3. B. SCHULTRICH and K. WETZIG, *J. Mater. Sci.* **22** (1987) 3361.
4. K. WETZIG, J. EDELMANN, W. FISCHER and H. MÜLLER, *Scanning* **9** (1987) 99.
5. W. HAUFFE and B. SCHULTRICH, *Prakt. Metall.* **25** (1988) 517.

6. R. HÜBEL, Private communication (1991).
7. W. DELLE, J. LINKE, H. NICKEL and E. WALLURA, "Spezielle Berichte der Kernforschungsanlage Jülich", No. 401, edited by K. F. A. Jülich and H.-A. Bahr (1987).
8. B. SCHULTRICH, H.-J. WEISS and H.-A. BAHR, in "Proceedings of the Workshop on Thermal Shock and Thermal Fatigue Behaviour of Advanced Ceramics", edited by G. A. Schneider and G. Petzow (Kluwer Academic, Dortrecht, 1993).

Received 10 March 1993
and accepted 22 April 1994